Unique Spin Vortices in Quantum Dots with Spin-orbit Couplings

Wenchen Luo,* Amin Naseri,† Jesko Sirker,‡ and Tapash Chakraborty§
Department of Physics and Astronomy, University of Manitoba, Winnipeg, Canada R3T 2N2
(Dated: February 2, 2018)

Spin textures of one or two electrons in a quantum dot with Rashba or Dresselhaus spin-orbit couplings reveal several intriguing properties. We show that even at the single-electron level spin vortices with different topological charges exist. These topological textures appear in the *ground state* of the dots. The textures are stabilized by time-reversal symmetry breaking and are robust against the eccentricity of the dot. The phenomenon persists for the interacting two-electron dot in the presence of a magnetic field.

A variety of topological states have recently been observed in condensed matter physics. These novel states of matter are a direct consequence of spin-orbit coupling (SOC) [1, 2] with topological insulators (TIs) being one of the most prominent examples [3, 4]. The SOC also plays an important role in tailoring topological superconductors (TSs) where the elusive Majorana fermions might be present [5–7]. Both TIs and TSs display a topologically non-trivial structure in momentum space. SOC can, however, also lead to topological charges in real space. The Dzyaloshinskii-Moriya interaction [8, 9]—microscopically based on the SOC—can, for example, give rise to spin skyrmions in helical magnets [10, 11] and pseudospin skyrmions in bilayer graphene [12]. Synthetic spin-orbit couplings can also be engineered in cold atomic gases and skyrmion-like spin textures have been observed [13, 14].

Quantum dots (QDs) are of practical and fundamental interest and provide an excellent platform to control the spin and charge of a single electron [15–22]. Extensive studies on QDs with SOCs have been reported in recent years [23–39]. Furthermore, a Berry connection [40] in momentum space induced by the SOC has been studied [35, 36].

In this letter, we investigate the spin textures associated with the electron density profiles in isotropic and elliptical QDs. We show that in the presence of SOC the in-plane spin texture of a single electron is a spin vortex. The QD is consequently turned into an artificial atom [41] with topological features. Spin vortices often emerge in many-spin systems forming either a crystalline arrangement or vortex/anti-vortex pairs [42, 43]. For instance, in quantum Hall systems the skyrmion is a single-particle excitation in low Landau levels and the in-plane spin texture is similar to the one we find in a QD with SOC. The skyrmion excitations in the former case are, however, induced by Coulomb interactions [44]. In contrast, we show here that in a QD a single vortex can exist in the ground-state of a non-interacting quantum system.

We focus on the physics of the two-dimensional (2D) surface where the QD is constructed [16]. We consider both the Rashba and the linear Dresselhaus SOCs which arise in materials with broken inversion symmetry. The strength of the Rashba SOC can be controlled by a gate electric field [45–49]. Moreover, the ratio of the Rashba SOC to the Dresselhaus SOC can be tuned over a wide range, for instance in InAs QDs, by applying an in-plane magnetic field [49]. We will show that this leads to a system where the topological charge can be dynamically controlled by external electromagnetic fields making spin vortices in QDs possible candidates for future spintronics and quantum information applications.

The SOCs can be theoretically considered as effective momentum-dependent magnetic fields [50–53]. In the absence of a confinement and an external magnetic field, the momentum is conserved and the SOC in the Hamiltonian becomes a momentum-dependent operator with a good quantum number (e.g., the helicity operator for Rashba SOC). On the other hand, the spin state is momentum-independent if both Rashba and Dresselhaus couplings have equal strength and there is no Zeeman coupling, leading to a persistent spin helix [54–56]. This particular spin state persists in the presence of a confinement potential and can be obtained by exactly solving the Hamiltonian which is equivalent to a quantum Rabi model [57]. If the spin is not a good quantum number then it is instructive to study the spin field in a given single-particle wavefunction $\Psi(\mathbf{r})$ of the dot

$$\sigma_i(\mathbf{r}) = \Psi^\dagger(\mathbf{r})\sigma_i\Psi(\mathbf{r}), \tag{1}$$

where σ_i for $i = x, y, z$ are Pauli matrices. An in-plane vector field $\boldsymbol{\sigma}(\mathbf{r}) = (\sigma_x(\mathbf{r}), \sigma_y(\mathbf{r}))$ reveals how the spin in real space is locally affected by the effective magnetic field. In the following, we demonstrate that generic SOCs compel the spin field to rotate around the center of the QD and to develop into a spin vortex.

The Hamiltonian of an electron with effective mass m^* and charge $-e$ in a quantum dot with SOCs is given by

$$H = \frac{(\mathbf{p}+e\mathbf{A})^2}{2m^*} + \frac{m^*}{2}\left(\omega_x^2x^2 + \omega_y^2y^2\right) + \frac{\Delta\sigma_z}{2} + H_{SOC}, \tag{2}$$

where the vector potential is chosen in the symmetric gauge $\mathbf{A} = \frac{1}{2}B\,(-y, x, 0)$ with the magnetic field B. The confinement is anisotropic with the frequencies in two directions, ω_x and ω_y, and Δ is the Zeeman coupling. We consider both the Rashba SOC, H_R, and the Dresselhaus SOC, H_D, with

$$H_R \;=\; g_1\left(\sigma_xP_y - \sigma_yP_x\right), \tag{3}$$

$$H_D \;=\; g_2\left(\sigma_y P_y - \sigma_x P_x\right), \tag{4}$$

and $H_{SOC} = H_R + H_D$. $P_i = p_i + eA_i$ is the kinetic momentum, and $g_{1,2}$ determine the strength of each SOC. We note that Rashba and Dresselhaus terms have different rotational symmetry generators, H_R commutes with $L_z + \hbar\sigma_z/2$ while H_D commutes with $L_z - \hbar\sigma_z/2$, where L_z is the z-component of the angular momentum operator. In the following, we will show that this difference is responsible for the different topological charges associated with the spin vortex of the dot.

It is also useful to introduce a renormalized set of frequencies $\Omega_i = \sqrt{\omega_i^2 + \omega_c^2/4}$ with the cyclotron frequency $\omega_c = eB/m^*$. The natural length scales in x and y directions are $\ell_i = \sqrt{\hbar/(m^*\Omega_i)}$ while the confinement lengths are defined as $R_i = \sqrt{\hbar/(m^*\omega_i)}$. In the numerical calculations presented in the following the eigenvectors of $H_0 = \frac{\mathbf{p}^2}{2m^*} + \frac{m^*}{2}\left(\Omega_x^2 x^2 + \Omega_y^2 y^2\right) + \frac{\Delta}{2}\sigma_z$, which is a two-dimensional harmonic oscillator, are used as a basis set.

No analytical solution is known for the generic Hamiltonian in Eq. (2) due to its complexity [58]. We can, however, analytically investigate the special case of an isotropic dot ($\Omega_{x,y} = \Omega$, $\ell_{x,y} = \ell$) without a magnetic field and with equal SOCs, $g_{1,2} = g$. The Hamiltonian (2) is then equivalent to a two-component quantum Rabi model which has been extensively studied in quantum optics [57]. The ground states in this case are a degenerate Kramers pair due to time reversal symmetry,

$$|GS\rangle_\pm = \frac{1}{\sqrt{2}} e^{\pm i\sqrt{2}m^*(y-x)g/\hbar} \begin{pmatrix} \pm e^{-i\pi/4} \\ 1 \end{pmatrix} |0,0\rangle \tag{5}$$

where $|0,0\rangle$ is the ground state of the two-dimensional quantum oscillator H_0. A very weak magnetic field will lift the degeneracy of the Kramers pair, and the unique ground state is then given by $|GS\rangle = (|GS\rangle_+ + \mathrm{sgn}(\Delta)\,|GS\rangle_-)/\sqrt{2}$ which minimizes the energy [57]. The spin fields are consequently well defined. We note some features of the spin field: (i) There is a mirror symmetry about the line $x = \pm y$. (ii) $\sigma_x(\mathbf{r}) + \sigma_y(\mathbf{r}) = 0$, and $\sigma_x(\mathbf{r}) = \sigma_y(\mathbf{r}) = 0$ along the line $x = y$. (iii) $\sigma_z(\mathbf{r}) = -\frac{\mathrm{sgn}(\Delta)}{\pi\ell^2} e^{-2x^2/\ell_x} \cos\left(4\sqrt{2}m^* x g/\hbar\right)$ along the line $x = -y$, i.e., $\sigma_z(\mathbf{r})$ is a spiral. Its period is related to the effective mass and the strength of the SOCs. We find that the exact solution perfectly agrees with the exact diagonalization results shown in Fig. 1. Similar results are found for the case $g_1 = -g_2$. For large magnetic fields the exact solution for the case without field is no longer a good starting point and the spin texture starts to rotate [57].

Next, we study the case of an isotropic dot in a weak magnetic field with generic strengths of the SOCs g_1 and g_2 based on a standard perturbative calculation. We find that the in-plane spin fields up to first order in $g_{1,2}$ are given by

$$\sigma_x(\mathbf{r}) \;=\; \xi(r)(r/\ell)\left(\bar{g}_2 \sin\theta - \bar{g}_1 \cos\theta\right), \tag{6}$$

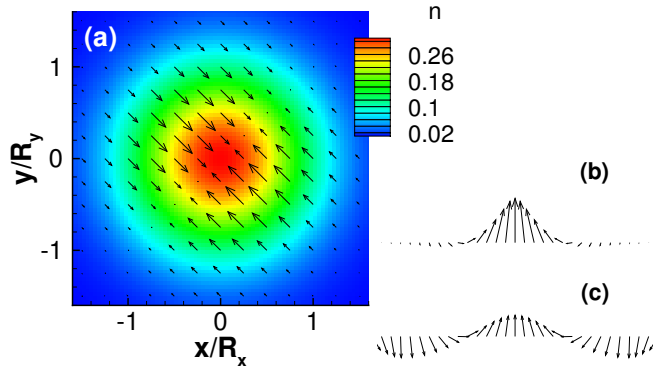

FIG. 1: (Color online) Numerical results for a single-electron QD with $R_x = R_y = 35$nm, $B = 0.1$T, and equal SOCs $\hbar g_1 = \hbar g_2 = 20$ nm$\cdot$ meV. (a) Electron density (contours) and in-plane spin fields (arrows), (b) $\sigma_z(\mathbf{r})$ along $x = -y$, and (c) the normalized $\tilde{\sigma}_z(\mathbf{r}) = \sigma_z(\mathbf{r})/\sqrt{\boldsymbol{\sigma}(\mathbf{r})^2 + \sigma_z(\mathbf{r})^2}$ along $x = -y$.

$$\sigma_y(\mathbf{r}) \;=\; \xi(r)(r/\ell)\left(\bar{g}_2 \cos\theta - \bar{g}_1 \sin\theta\right), \tag{7}$$

and $\sigma_z(\mathbf{r}) = \xi(r)/2$ with $\xi(r) = 2e^{-r^2/\ell^2}/\pi\ell^2$, θ is the polar angle in coordinate space, and the new parameters are

$$\bar{g}_{1,2} = \frac{\hbar g_{1,2}}{\ell} \frac{1 \pm \omega_c/(2\Omega)}{\hbar(\Omega \pm \omega_c/2) - \Delta}, \tag{8}$$

where we have assumed $\Delta < 0$. The in-plane spin field $\sigma(\mathbf{r})$ winds once around the origin and acquires a topological charge $q = \pm 1$ when $\bar{g}_1 \neq \bar{g}_2$. If $\bar{g}_1 = \bar{g}_2$, no vortex appears in agreement with the exact solution discussed earlier. If $g_1 = 0$ or $g_2 = 0$, $\sigma(\mathbf{r})$ obtained perturbatively qualitatively agrees with the numerical solutions shown in Fig. 2, and the vortices even exist in a strong magnetic field beyond the perturbation calculations. We

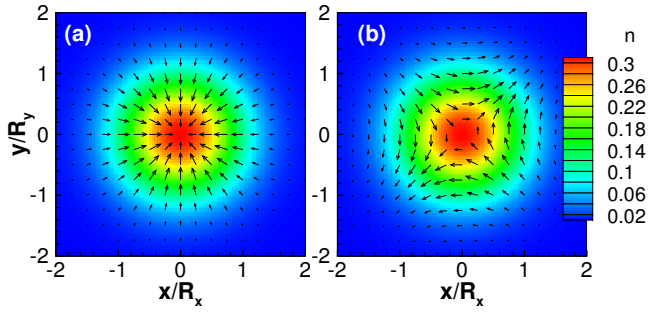

FIG. 2: (Color online) Single-electron QD with $R_x = R_y = 15$nm, $B = 0.1$T ($\Delta < 0$), and (a) Rashba SOC $\hbar g_1 = 40$ nm$\cdot$ meV only, and (b) Dresselhaus SOC $\hbar g_2 = 20$ nm$\cdot$ meV only.

stress that the two vortex configurations are stable and representative for the regime $g_1 \gg g_2$ and $g_2 \gg g_1$, respectively [57]. We further note that under $B \to -B$ the spin field changes direction, $\sigma(\mathbf{r}) \to -\sigma(\mathbf{r})$, leaving the topological charge invariant though.

Next, we analyze the rotational symmetry of the two types of SOCs in order to characterize the sign of the winding number. First, we consider the spin field of a dot when only the Rashba SOC is present. The spin field is then invariant under the rotation matrix

$$U_R(\vartheta) = \begin{pmatrix} \cos\vartheta & \sin\vartheta \\ -\sin\vartheta & \cos\vartheta \end{pmatrix}, \tag{9}$$

for $\vartheta \in [0, 2\pi]$, which is rooted in the rotational symmetry of a Rashba dot under the operator $L_z + \hbar\sigma_z/2$. Therefore, the in-plane spin rotates clockwise by 2π if we move around the center of the dot in a clockwise direction, and hence, its winding number is $q = +1$. On the other hand, the in-plane spin field of a dot with only Dresselhaus SOC being present, is invariant under the action of $U_D(\vartheta) = U_R(-\vartheta)$. Along the same line of reasoning, the in-plane spin field then rotates anticlockwise by 2π if we move around the center in a clockwise direction. Dresselhaus SOC thus leads to a winding number $q = -1$. In the absence of an external magnetic field B, Kramers degeneracy may cancel the spin textures, since there is a global π phase difference between the pair. Hence, the vortices should be stabilized by breaking of time-reversal symmetry.

In summary, we find for the single-electron dot with $g_1 = \pm g_2$ and without or in a very weak magnetic field, that the in-plane spin field does not form a vortex. There is, however, a spiral in $\sigma_z(\mathbf{r})$ along the line $x = \mp y$. For dominant Rashba or Dresselhaus SOC, on the other hand, the exact diagonalization results clearly show the formation of spin vortices. Rashba SOC induces a vortex with topological charge $q = +1$ while the Dresselhaus SOC induces a vortex with $q = -1$. These topological charges associated with the spin textures are stabilized by time-reversal symmetry breaking and are robust against the ellipticity of the dot [57]. If the dot is strained, the topological features are not changed, since the spin textures originate from the SOCs of the material. The total $\langle\sigma_z\rangle$ in the presence of SOC is no longer constant as a function of the applied magnetic field and becomes more and more polarized with increasing magnetic field. In Fig. 3 we compare $\langle\sigma_z\rangle$ for different cases. The distinct behavior of $\langle\sigma_z\rangle$ when SOCs are present might be observable experimentally via magnetometry or optically pumped NMR measurements [59, 60].

If there is more than one electron confined in the dot, we need to also consider the Coulomb interaction. The Hamiltonian of the interaction is given by $H_C = V(n_1, n_2, n_3, n_4)\, c^\dagger_{n_1} c^\dagger_{n_2} c_{n_3} c_{n_4}$, where c is the electron annihilation operator and $n_i = (n_{ix}, n_{iy}, n_s)$ is an index combining the quantum numbers of the two-dimensional oscillator in x, y direction with the spin index. The interaction matrix elements are given in the Suppl. Mat. [57]. The full Hamiltonian with interaction is then $H_I = H + H_C$ with H as given in Eq. (2). We diagonalize the interacting Hamiltonian exactly to obtain the

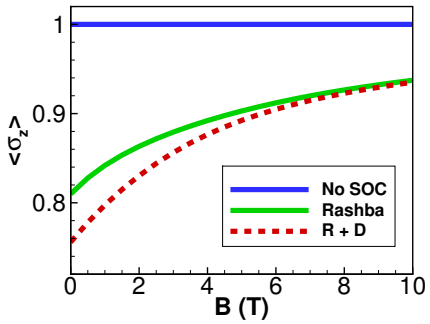

FIG. 3: (Color online) The total $\langle\sigma_z\rangle$ in a single-electron dot ($R_x = R_y = 15$nm) without SOC, with Rashba SOC only ($\hbar g_1 = 40$ nm· meV), and with both Rashba and Dresselhaus SOCs ($\hbar g_1 = 40$ nm· meV, $\hbar g_2 = 20$ nm· meV).

electron and spin densities. Since the interacting system does contain very rich physics, we restrict the discussion in the following to the case of a dot with two electrons. To be concrete, we consider the case of an InAs dot here, where the effective mass is $m^* = 0.042 m_e$, Landé factor $g_L = -14$ and dielectric constant $\epsilon = 14.6$. In this system it appears to be experimentally feasible to change the ratio of the SOCs g_1/g_2 over a wide range.

In a two-electron dot with Coulomb interactions, the spin textures can be much more complex than in the single-electron case. If there is no time reversal symmetry breaking, the texture is cancelled by the Kramers pair. In the presence of a magnetic field, the spin textures appear again with topological charge $+1$ or -1 if the dot is perfectly isotropic. For an anisotropic quantum dot the electron density will split into two centers in a strong magnetic field even without SOC. With SOCs the spin textures are modified by this density deformation. In the examples shown in Fig. 4, we find in both cases three vortices along the elongated x axis. In the Rashba SOC case shown in Fig. 4(a) there are two vortices with $q = 1$ and one with $q = -1$, while there are two vortices with $q = -1$ and one with $q = 1$ in the Dresselhaus SOC case presented in Fig. 4(b). Hence, the total winding numbers are still $+1$ and -1 in a Rashba SOC and Dresselhaus SOC system, respectively, as in the single-electron dot. Indeed, the spin textures along the edges of the dot are quite similar to the single-particle case. Here interactions are less relevant and the spin textures are thus mainly induced by the SOCs.

In an isotropic two-electron dot with equal SOCs, $g_1 = g_2$, we find that both the density profiles and spin textures undergo a dramatic change as a function of the applied magnetic field [Fig. 5]. In this case, the spin and density profiles are determined collectively by *both* the interactions and SOCs. For large magnetic fields we find, in particular, that the electron density splits mirror symmetrically along the line $x = y$ [Fig. 5(b)], causing also

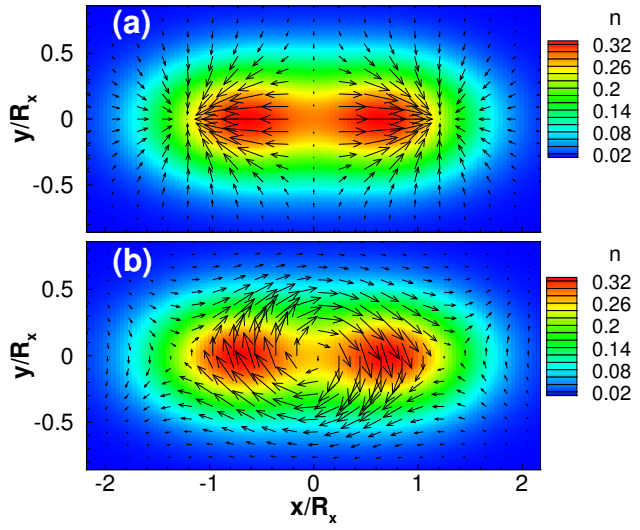

FIG. 4: (Color online) The in-plane spin fields in an elliptic dot with two electrons, $R_x = 15$nm, $R_y = 10$nm at $B = 5$T. The colors represent the electron density. (a) Rashba SOC only with $\hbar g_1 = 40$ nm· meV, and (b) Dresselhaus SOC only with $\hbar g_2 = 20$ nm· meV.

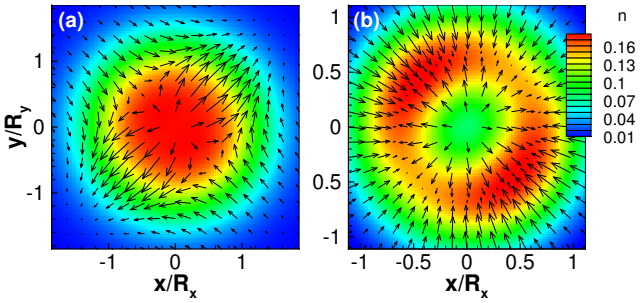

FIG. 5: (Color online) The in-plane spin fields in a two-electron dot with $R_x = R_y = 15$nm, and $\hbar g_1 = \hbar g_2 = 20$ nm ·meV. The colors represent the electron density. (a) $B = 3.5$T, topological charge $q = -1$, and (b) $B = 18$T leading to $q = +1$.

a complete rearrangement of the associated spin texture and a change of the total topological charge. This has to be contrasted with the case of an InAs dot without SOC where the angular momentum of the ground state changes from $L = -1$ to $L = 3$ at about $B = 17$T leading instead to a ring-shaped electron density. We further note that in a ZnO dot with stronger Coulomb interaction [61], the splitting of the electron density and the spin textures can be generated in a much lower magnetic field. Details will be published elsewhere. This splitting—which only occurs if both interactions and SOCs are present—could possibly be observed experimentally and would thus provide an indirect confirmation of a non-trivial spin texture in the dot.

In summary, we find that the combination of electron confinement and SOCs leads to vortex-like spin textures in the ground state even for a single-electron dot. The spin texture can be stabilized by an external magnetic field breaking the time-reversal symmetry. Interestingly, the winding number of the vortex is different for dots with dominant Rashba SOC or Dresselhaus SOC. This difference can be traced back to the different symmetries of the Hamiltonian. The Rashba SOC commutes with $L_z + \hbar\sigma_z/2$ leading to a topological charge of the spin field of $q = +1$ while the Dresselhaus SOC commutes with $L_z - \hbar\sigma_z/2$ and the topological charge is $q = -1$. Using the exact diagonalization scheme we have shown that these spin vortices do persist also in interacting multi-electron dots. For an elliptic two-electron dot we find, in particular, that more than one spin vortex can exist. In all investigated cases the total topological charge is, however, still $q = \pm 1$ as in the single-electron case. Physically, this is understood by noting that the spin configuration at the edge of the dot, where the electron density is low, is only weakly affected by the interactions. We thus conjecture that the total topological charge for a spin texture in multi-electron dots is always fixed to $q = \pm 1$.

The spin textures in QDs described in this letter are similar to the in-plane structure of (anti-)skyrmion excitations in quantum Hall systems. The locations of the skyrmions in a quantum Hall systems are, however, unknown making it difficult to observe a single skyrmion directly. The existence of skyrmions has so far only been confirmed indirectly by NMR and transport measurements. In contrast, the spin vortices in QD systems are localized at a known position. This might possibly open new avenues for spintronics and quantum information applications. Arrays of QDs have, for example, been realized experimentally [62, 63] and have been considered as a potential platform for quantum computation [64–67]. In such an array of QDs with SOCs the ratio of Rashba to Dresselhaus couplings might be tunable by gates over a sufficiently wide range to realize a system with localized and controllable topological charges $q = \pm 1$. At a minimum, such a setup would allow for an indirect probe of the spin texture by measuring the field dependence of the out-of-plane spin component [Fig. 3], either by a magnetometer or in an NMR experiment [60].

We acknowledge useful discussions with Sean Barrett (Yale). TC acknowledges support by the Canada Research Chairs Program of the Government of Canada. JS acknowledges support by the Natural Sciences and Engineering Research Council (NSERC, Canada) and by the Deutsche Forschungsgemeinschaft (DFG) via Research Unit FOR 2316. Computation time was provided by Calcul Québec and Compute Canada.

* Electronic address: wenchen.luo@umanitoba.ca

† Electronic address: naserija@umanitoba.ca
‡ Electronic address: sirker@physics.umanitoba.ca
§ Electronic address: Tapash.Chakraborty@umanitoba.ca

[1] A. Manchon, H. C. Koo, J. Nitta, S. M. Frolov, and R. A. Duine, Nat. Mater. **14**, 871-882 (2015).
[2] Y. Ren, Z. Qiao, and Q. Niu, Rep. Prog. Phys. **79**, 066501 (2016).
[3] M. Z. Hasan, and C. L. Kane, Rev. Mod. Phys. **82**, 3045 (2010).
[4] X. L. Qi and S. C. Zhang, Rev. Mod. Phys. **83**, 1057 (2011).
[5] J. Alicea, Rep. Prog. Phys. **75**, 076501 (2012).
[6] V. Mourik, K. Zuo, S. M. Frolov, S. R. Plissard, E. P. A. M. Bakkers, L. P. Kouwenhoven, Science **336**, 1003-1007 (2012).
[7] M. Sato, and Y. Ando, Rep. Prog. Phys. **80**, 076501 (2017).
[8] I. E. Dzyaloshinskii, J. Phys. Chem. Solids **4**, 241 (1958).
[9] T. Moriya, Phys. Rev. **120**, 91 (1960).
[10] S. Mühlbauer, B. Binz, F. Jonietz, C. Pfleiderer, A. Rosch, A. Neubauer, R. Georgii, P. Böni, Science **323**, 915-919 (2009).
[11] X. Z. Yu, Y. Onose, N. Kanazawa, J. H. Park, J. H. Han, Y. Matsui, N. Nagaosa, and Y. Tokura, Nature **465**, 901-904 (2010).
[12] R. Côté, Wenchen Luo, Branko Petrov, Yafis Barlas, and A. H. MacDonald Phys. Rev. B **82**, 245307 (2010); R. Côté, J. P. Fouquet, and Wenchen Luo, Phys. Rev. B **84**, 235301 (2011).
[13] H. Hu, B. Ramachandhran, H. Pu, and X.-J. Liu, Phys. Rev. Lett. **108**, 010402 (2012).
[14] R. M. Wilson, B. M. Anderson, and C. W. Clark, Phys. Rev. Lett. **111**, 185303 (2013).
[15] T. Chakraborty, Quantum Dots (Elsevier, Amsterdam, 1999).
[16] D. Bimberg, M. Grundmann, and N. N. Ledentsov, Quantum Dot Heterostructures (John Wiley and Sons, Chichester, 1999).
[17] D. Loss and D. P. DiVincenzo, Phys. Rev. A **57**, 120 (1998).
[18] L. P. Kouwenhoven, D. G. Austing, and S. Tarucha, Rep. Prog. Phys. **64**, 701-736 (2001).
[19] R. Hanson, L. P. Kouwenhoven, J. R. Petta, S. Tarucha, and L. M. K. Vandersypen, Rev. Mod. Phys. **79**, 1217 (2007).
[20] C. Kloeffel, and D. Loss, Annu. Rev. Condens. Matter Phys. **4**, 51 (2013).
[21] A. J. Bennett, M. A. Pooley, Y. Cao, N. Sköld, I. Farrer, D. A. Ritchie, and A. J. Shields, Nat. Comm. **4**, 1522 (2013).
[22] R. J. Warburton, Nat. Mater. **12**, 483 (2013).
[23] O. Voskoboynikov, C. P. Lee, and O. Tretyak, Phys. Rev. B **63**, 165306 (2001).
[24] M. Governale, Phys. Rev. Lett. **89**, 206802 (2002).
[25] A. Emperador, E. Lipparini, and F. Pederiva, Phys. Rev. B **70**, 125302 (2004).
[26] D. V. Bulaev, and D Loss, Phys. Rev. B **71**, (2005).
[27] S. Weiss and R. Egger, Phys. Rev. B **72**, 245301 (2005).
[28] T. Chakraborty, and P. Pietiläinen, Phys. Rev. Lett. **95**, 136603 (2005); P. Pietiläinen, and T. Chakraborty, Phys. Rev. B **73**, 155315 (2006).
[29] A. Ambrosetti, F. Pederiva, and E. Lipparini, Phys. Rev. B **83**, 155301 (2011).
[30] C. F. Destefani, S. E. Ulloa, and G. E. Marques, Phys. Rev. B **69**, 125302 (2004).
[31] T. Chakraborty, and P. Pietiläinen, Phys. Rev. B **71**, 113305 (2005).
[32] A. Cavalli, F. Malet, J. C. Cremon, and S. M. Reimann, Phys. Rev. B **84**, 235117 (2011).
[33] A. Naseri, A. Zazunov, and R. Egger, Phys. Rev. X **4**, 031033 (2014).
[34] S. Avetisyan, P. Pietiläinen, and T. Chakraborty, Phys. Rev. B **88**, 205310 (2013).
[35] S. Avetisyan, T. Chakraborty, and P. Pietiläinen, Physica E **81**, 334 (2016).
[36] S. K. Ghosh, Jayantha P. Vyasanakere, and V. B. Shenoy, Phys. Rev. A **84**, 053629 (2011).
[37] Yi Li, Xiangfa Zhou, and Congjun Wu, Phys. Rev. B **85**, 125122 (2012).
[38] Siranush Avetisyan, Pekka Pietiläinen, and Tapash Chakraborty, Phys. Rev. B **88**, 205310 (2013).
[39] S. D. Ganichev, V. V. Bel'kov, L. E. Golub, E. L. Ivchenko, Petra Schneider, S. Giglberger, J. Eroms, J. De Boeck, G. Borghs, W. Wegscheider, D. Weiss, and W. Prettl, Phys. Rev. Lett. **92**, 256601 (2004).
[40] D. Xiao, M.-C. Chang, and Q. Niu, Rev. Mod. Phys. **82**, 1959 (2010).
[41] P.A. Maksym, and T. Chakraborty, Phys. Rev. Lett. **65**, 108 (1990).
[42] J. M. Kosterlitz, and D. J. Thouless, J. Phys. C: Solid State Phys. **6**, (1973).
[43] P. Milde, D. Köhler, J. Seidel, L. M. Eng, A. Bauer, A. Chacon, J. Kindervater, S. Mühlbauer, C. Pfleiderer, S. Buhrandt, C. Schütte, A. Rosch, Science **340**, 1076-1080 (2013).
[44] Z. F. Ezawa, Quantum Hall Effects: Field Theoretical Approach and Related Topics (World Scientific, 2000).
[45] J. Nitta, T. Akazaki, H. Takayanagi, and T. Enoki, Phys. Rev. Lett. **78**, 1335 (1997).
[46] M. Kohda, T. Bergsten, and J. Nitta, J. Phys. Soc. Jpn. **77**, 031008 (2008).
[47] C. R. Ast, D. Pacilé, L. Moreschini, M. C. Falub, M. Papagno, K. Kern, M. Grioni, J. Henk, A. Ernst, S. Ostanin, and P. Bruno, Phys. Rev. B **77**, 081407(R) (2008).
[48] Y. Kanai, R. S. Deacon, S. Takahashi, A. Oiwa, K. Yoshida, K. Shibata, K. Hirakawa, Y. Tokura, and S. Tarucha, Nat. Nanotechnol. **6**, 511 (2011).
[49] M. P. Nowak, B. Szafran, F. M. Peeters, B. Partoens, and W. J. Pasek, Phys. Rev. B **83**, 245324 (2011).
[50] E. I. Rashba, Fiz. Tverd. Tela **2**, 1224 (1960); [Sov. Phys. Solid State **2**, 1109 (1960)].
[51] G. Dresselhaus, Phys. Rev. **100**, 580 (1955).
[52] R. Winkler, Spin-Orbit Coupling Effects in Two-Dimensional Electron and Hole Systems (Springer-Verlag, Berlin, 2003).
[53] G. Bihlmayer, O. Rader, and R. Winkler, New J. Phys. **17**, 050202 (2015).
[54] J. Schliemann, J. C. Egues, and D. Loss, Phys. Rev. Lett. **90**, 146801 (2003).
[55] B. A. Bernevig, J. Orenstein, and S.-C. Zhang, Phys. Rev. Lett. **97**, 236601 (2006).
[56] J. D. Koralek, C. P. Weber, J. Orenstein, B. A. Bernevig, S.-C. Zhang, S. Mack, and D. D. Awschalom, Nature **458**, 610 (2009).
[57] See the supplementary material for details.
[58] A QD with a hard-wall confinement allows for an exact analytical solution in the presence of either Rashba or Dresselhaus SOC: E. Tsitsishvili, G. S. Lozano, and A.

O. Gogolin, Phys. Rev. B **70**, 115316 (2004).
[59] A.E. Dementyev, P. Khandelwal, N. N. Kuzma, S.E. Barrett, L. N. Pfeiffer, K. W. West, Solid State Comm. **119**, 217 (2001); N. N. Kuzma, P. Khandelwal, S. E. Barrett, L. N. Pfeiffer, K. W. West, Science **281**, 686 (1998); S. E. Barrett, G. Dabbagh, L. N. Pfeiffer, K. W. West, and R. Tycko, Phys. Rev. Lett. **74**, 5112 (1995).
[60] S.E. Barrett, Private communications (2017).
[61] T. Chakraborty, A. Manaselyan, and M. Barseghyan, J. Phys.:Condens. Matter **29**, 215301 (2017).
[62] L. P. Kouwenhoven, F. W. J. Hekking, B. J. van Wees, C. J. P. M. Harmans, C. E. Timmering, and C. T. Foxon, Phys. Rev. Lett. **65**, 361 (1990).
[63] I. Piquero-Zulaica, J. Lobo-Checa, A. Sadeghi, Z.M. Abd El-Fattah, Ch. Mitsui, T. Okamoto, R. Pawlak, T. Meier, A. Arnau, J. E. Ortega, Jun Takeya, S. Goedecker, E. Meyer, and S. Kawai, Nat. Comm. **8**, 787 (2017).
[64] Daniel Loss and David P. DiVincenzo, Phys. Rev. A **57**, 120 (1998).
[65] Paolo Zanardi and Fausto Rossi, Phys. Rev. Lett. **81**, 4752 (1998).
[66] D. D. Awschalom, L. C. Bassett, A. S. Dzurak, E. L. Hu, and J. R. Petta, Science **339**, 1174 (2013).
[67] K. C. Nowack, F. H. L. Koppens, Y. V. Nazarov, L. M. K. Vandersypen, Science **318**, 1430 (2007).